JPE 4-3-5

AC and DC Applications of Induction Generator Excited by Static VAR Compensator

Tarek Ahmed†, Katsumi Nishida* and Mutsuo Nakaoka*

The Graduate School of Science and Engineering, Yamaguchi University, Yamaguchi, Japan

ABSTRACT

This paper presents the steady-state analysis of the three-phase self-excited induction generator (SEIG). The three-phase SEIG with a squirrel cage rotor is driven by a variable-speed prime mover (VSPM) or a constant-speed prime mover (CSPM) such as a wind turbine or a micro gas turbine. Furthermore, a PI closed-loop feedback voltage regulation scheme of the three-phase SEIG driven by a VSPM on the basis of the static VAR compensator (SVC) is designed and evaluated for the stand-alone AC and DC power applications. The simulation and experimental results prove the practical effectiveness of the additional SVC with the PI controller-based feedback loop in terms of its fast responses and high performances

Keywords: Self-excited induction generator, Static VAR compensator, Terminal Voltage Control

1. Introduction

Over the past twenty years, many researchers have analyzed the steady-state performances of the three-phase SEIG on the basis of its approximate equivalent circuit. The steady-state analysis of the three-phase SEIG driven by a constant-speed prime mover (CSPM) uses the nodal admittance approach and the series impedance approach with the following reasonable assumptions: [1-3]

- Iron losses are negligible.
- Only fundamental M.M.F. waves are considered.
- Resistances and reactances of the three-phase induction machine are constant, except for the magnetizing reactance.
- The rate of change in the parameters and variables of the equivalent circuit is extremely small, so that the steady-state equivalent circuit can be used.

Using an iterative technique, the steady-state analysis of the three-phase SEIG driven by a variable-speed prime mover (VSPM) has been carried out in reference[4]. All parallel branches of the three-phase SEIG approximate equivalent circuit are converted to its equivalent series branches. This technique cannot be applied for the steady-state analysis of the single-phase SEIG driven by a VSPM[5].

The terminal voltage of the three-phase SEIG with variable loads can be maintained at a constant value by adjusting the value of the excitation capacitance or by controlling the prime mover speed. Adjustment of prime mover speed is not always possible. Therefore, the appropriate method is keeping the adjustment of the capacitor value continuous. The adjustable excitation capacitor value can be achieved by many control strategies

Manuscript received Jan.26, 2004; revised May 30, 2004.
†Corresponding Author: tarek@pe-news1.eee.yamaguchi-u.ac.jp
Tel: +81-836-85-9472, Fax: +81-836-85-9401,Yamaguchi Univ.
*The Graduate School of Science and Eng., Yamaguchi Univ.

using power electronic technology[6-12]. Some of these proposals use inverters and field-orientation algorithms to excite and control the induction generator. That enables stiff voltage regulation and high efficiency. As a drawback, the field orientation requires costly and unreliable mechanical position sensing systems as encoders or resolvers. There are other proposals that do not require position-sensing systems. Some of them are based on a shunt-connected PWM voltage source inverter, supplying constant frequency voltage, and some others supplying the reactive current to the induction generator by a capacitor bank and an inverter simultaneously based on the instantaneous reactive power theory[11]-[12]. The voltage regulation of the three-phase SEIG driven by a CSPM using static VAR compensator (SVC) of the thyristor controlled reactor (TCR) with a fixed capacitor(FC) has been presented as an experimental work in reference[6].

This paper describes an effective algorithm for evaluating the steady-state performance analysis of the three-phase SEIG driven by a VSPM or a CSPM based on its equivalent circuit as a promising stand-alone power supply in a rural district. In addition, the simulation and experimental results of the closed-loop feedback with the PI controller, using the SVC for the terminal voltage regulation of the three-phase SEIG driven directly by the VSPM, are established and discussed for the stand-alone AC and DC utilizations.

2. System Description

The schematic system diagram of the three-phase SEIG voltage regulation, based on the SVC controlled by a PI controller in the feedback loop, is shown in Fig.1. The three-phase SEIG is excited by the SVC composed of the TCR in parallel with the thyristor switched capacitor(TSC) and the FC. The generated output voltage of the induction generator can be directly connected to the load facility installation and equipment that are non-sensitive to the AC frequency. These include an electric heater, a battery charger, battery energy storage, and super capacitor energy storage using a rectifier circuit as shown in Fig.1. Table 1 indicates the design specifications with the parameters of three-phase SEIG and the constant circuit parameters of the proposed voltage regulation system.

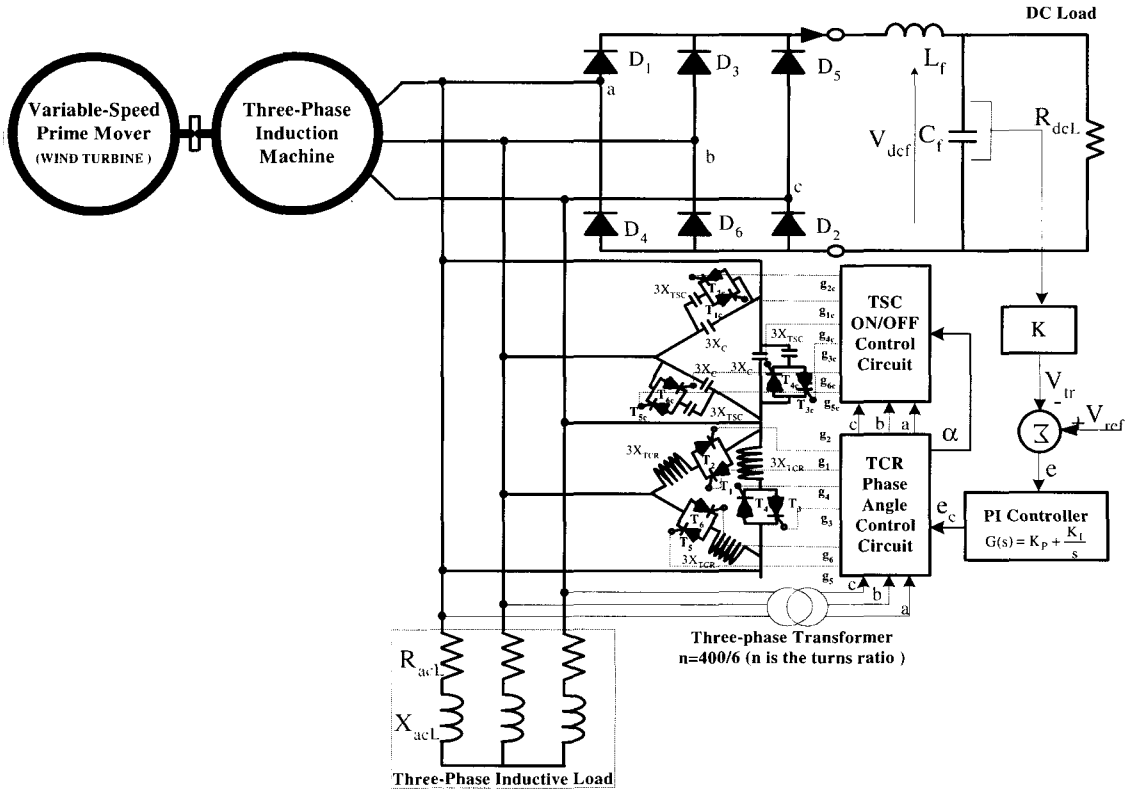

Fig.1 Schematic system configuration of three-phase SEIG with Static VAR compensator for AC and DC applications.

Table 1. Design Specifications and Circuit Parameters.

Items	*Machine Rating and Machine Parameters*	
Three-Phase Star Connected Induction Machine with Squirrel Cage Rotor	Rated Voltage	220 V
	Rated Power	2 kW
	Number of Poles	4
	Induction Machine Parameters at 50 Hz	
	R_1=0.517 ohm	X_1=1.0063 ohm
	R_2=0.517 ohm	X_2=1.0063 ohm
SVC composed of FC, TCR &TSC	X_{TCR} at 50 Hz; L_{TCR}	20 ohm, 0.064 H
	X_C at 50 Hz; C	13 ohm, 244 μF
	X_{TSC} at 50 Hz; C_{TSC}	64 ohm, 50 μF
PI Controller	K_P	0.38
	K_I	12.5
Low Pass Filter	C_F	2000 μF
	L_F	100 mH
VSPM (dc Motor)	τ_o	120
	υ_o	133

3. Variable-Speed Prime Mover Characteristics

The mechanical output power P_m of the VSPM is defined as [4]-[5],

$$P_m = (\tau_o - \upsilon_o \upsilon)\omega_s \upsilon \quad (1)$$

where $\upsilon(\upsilon=N/N_s)$ is the per unit speed of the VSPM, N and N_s are the rotor speed and the three-phase SEIG rated synchronous speed in rpm, respectively. ω_s is the rated synchronous angular speed. τ_o and υ_o respectively are the torque - speed coefficients of the VSPM characteristics. In experiment, a controllable dc motor is used with a constant armature voltage and a field current control. Fig.2 illustrates the effect of the field current control on the torque-speed characteristics of the VSPM.

4. Static VAR Control with PI Controller for Three-Phase SEIG Voltage Regulation

The fundamental component of the inductive current through the TCR is defined as[5]-[13],

$$I_{TCRf} = B_{TCR}(\sigma)V_t \quad (2)$$

The equivalent inductive susceptance $B_{TCR}(\sigma)$ is given by[13],

$$B_{TCR}(\sigma) = \frac{\sigma - \sin\sigma}{\pi X_{TCR}} \quad (3)$$

where X_{TCR} is the per-phase reactance of the TCR.

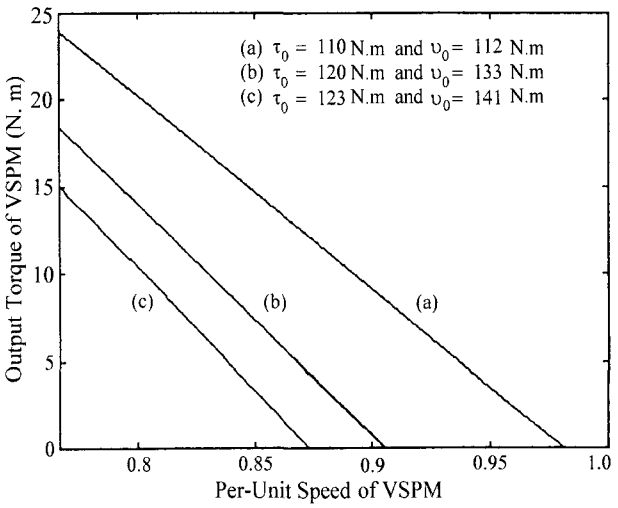

Fig.2. Torque-speed characteristics of VSPM.

The relationship between the conduction angle σ and the thyristor triggering delay angle α is[13],

$$\alpha + \frac{\sigma}{2} = \pi \quad (4)$$

The TSC is switched on when the rms terminal voltage of the SEIG is less than the rms reference voltage(220 V) and the triggering delay angle α of the TCR α=π.

The output signal $E_c(s)$ of the PI controller expressed in the discrete form is indicated by,

$$E_c(k) = E_c(k-1) + (K_p + T_s K_I)[V_{ref}(k) - V_{tr}(k)] - K_P[V_{ref}(k-1) - V_{tr}(k-1)] \quad (5)$$

where $[V_{ref}(k)-V_{tr}(k)]$ is the voltage error at sampling time k, $[V_{ref}(k-1)-V_{tr}(k-1)]$ is the error signal at sampling time (k-1), T_s is the sampling period. K_P and K_I are the Proportional and Integral gains of the PI controller, respectively.

5. Steady State Analysis of Three-Phase SEIG with Static VAR Compensator

The per-phase approximate equivalent circuit of the three-phase SEIG, excited by the SVC, is depicted in Fig.3[4]. The equivalent susceptance $B_{TCR}(\sigma)$ of the TCR and the capacitive reactance X_{TSC} of the TSC are connected in parallel with the fixed excitation reactance X_C[5]. The term (f-υ) is extremely small. As a result, the term (X_2^2) could be substantially neglected as compared

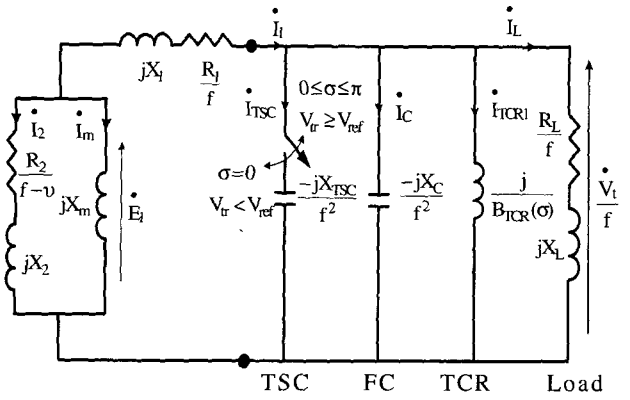

Fig.3. Per-phase approximate equivalent circuit of three-phase SEIG excited by SVC(FC,TCR & TSC) in steady state.

with $[R_2^2/(f-\upsilon)^2]$. The mechanical input power P_i of SEIG can be written as,

$$P_i = -3\frac{E_1^2}{R_2}\left(\frac{f-\upsilon}{f}\upsilon\right) \tag{6}$$

where E_1 is the air gap voltage per phase, R_2 and X_2 are the resistance and leakage reactance of the rotor winding used in the SEIG stator winding, respectively. f is the per unit frequency (f=F/50.0, F is the output frequency of the SEIG).

By making a mechanical power balance through equating Equation (6) to Equation (1). The per unit speed υ can be obtained as follows:

$$\upsilon = \frac{R_2\omega_s\tau_0 + 3E_1^2}{R_2\omega_s\upsilon_0 f + 3E_1^2} f \tag{7}$$

By applying the impedance approach on the per-phase approximate equivalent circuit of the SEIG with SVC shown in Fig.3, the following equation can be defined as,

$$\dot{Z}_{rm} + \dot{Z}_{mq} + \dot{Z}_{qr} = 0 \tag{8}$$

where $\dot{Z}_{rm}$, $\dot{Z}_{mq}$ and $\dot{Z}_{qr}$ are described by considering the equivalent circuit shown in Fig.3 and defined as (A1), (A2) and (A3), respectively in Appendix.

The two non-linear simultaneous equations of the magnetizing reactance X_m are obtained by equating the imaginary and real parts of Equation (8) to zero and arranged as follows,

$$X_m = -\frac{C_0 + C_1 f + C_2 f^2 + C_3 f^3 + C_4 f^4 + C_5 f^5}{A_0 + A_1 f + A_2 f^2 + A_3 f^3 + A_4 f^4 + A_5 f^5} \tag{9}$$

$$X_m = \frac{D_0 + D_1 f + D_2 f^2 + D_3 f^3 + D_4 f^4 + D_5 f^5}{(B_0 + B_1 f + B_2 f^2 + B_3 f^3) f^2} \tag{10}$$

Through equating Equation (9) and Equation (10), the 10^{th} degree polynomial equation is derived by,

$$Y_{10}f^{10} + Y_9 f^9 + Y_8 f^8 + Y_7 f^7 + Y_6 f^6 + Y_5 f^5 + Y_4 f^4 + Y_3 f^3 + Y_2 f^2 + Y_1 f + Y_0 = 0 \tag{11}$$

where the real coefficients from Y_0 to Y_{10} expressed in terms of constants A_i (i=0~5), B_j (j=0~3) , C_k (k=0~5) and D_l (l=0~5) are indicated in Appendix.

The per-unit frequency f can be determined from Equation(11) by using the Newton Raphson method with the initial value(τ_0/υ_0). By substituting the per-unit frequency f into Equation (9) or Equation (10), the magnetizing reactance X_m can be estimated. The air gap voltage E_1 is evaluated from the magnetization characteristic, which is the relationship between the air gap voltage E_1 and the magnetizing reactance X_m[5]. The magnetization curve obtained from the no-load test is expressed by,

$$E_1 = \begin{cases} 207.2 - 3.77X_m & X_m \le 24.2 \\ 541.7 - 17.79X_m & 24.2 \le X_m \le 26.5 \\ 0 & X_m \ge 26.5 \end{cases} \tag{12}$$

The SEIG performances can be evaluated by using its per-phase approximate equivalent circuit shown in Fig.3.

6. Simulation and Experimental Results

6.1 Operating performances of SEIG with VSPM

The steady-state analysis of the three-phase SEIG driven with a VSPM is derived by neglecting the per-phase equivalent inductive susceptance [$B_{TCR}(\sigma)$=0] of the TCR and the TSC capacitive reactance (X_{TSC}=0). A feasible prototype of the three-phase SEIG driven directly by a VSPM represented by a separately controlled excited dc motor is built and tested. Fig.4 shows the no-load generated terminal voltage vs. the excitation capacitance, which is above the minimum value required to build up

he terminal voltage of the three-phase SEIG driven by a VSPM. The terminal voltage of the three-phase SEIG driven by a VSPM with a certain torque-speed characteristic (τ_0=120, υ_0=133) increases with the excitation capacitance and also by increasing the prime mover speed by changing the torque-speed characteristic from (τ_0=120, υ_0=133) to (τ_0=110, υ_0=112) as illustrated in Fig.2. Fig.5 indicates the variations of the output frequency of the three-phase SEIG driven by a VSPM against its excitation capacitance at no load with different torque-speed characteristics. The output frequency of the three-phase SEIG decreases by increasing the excitation capacitance from 150 μF to 350 μF at certain torque-speed coefficients (τ_0=120, υ_0=133 where the VSPM speed decreases in accordance with the torque-speed characteristic of the VSPM shown in Fig.2) and increases linearly by increasing the speed as with other torque-speed coefficients (τ_0=110, υ_0=112). For an inductive load with a 0.8 lagging power factor, a specified torque-speed coefficients (τ_0=120, υ_0=133) and various excitation capacitances (C=194 μF, 244 μF, and 294 μF per phase), Fig.6 illustrates the induction generator terminal voltage variations with the inductive load power calculated from the simulation and experimental results. Fig.7 represents the VSPM speed variations due to the inductive load power changes vs. the terminal voltage of the three-phase SEIG. Fig.6 and Fig.7 indicate that the terminal voltage and the prime mover speed decrease as the inductive load power increases in accordance with the torque-speed characteristic of the VSPM

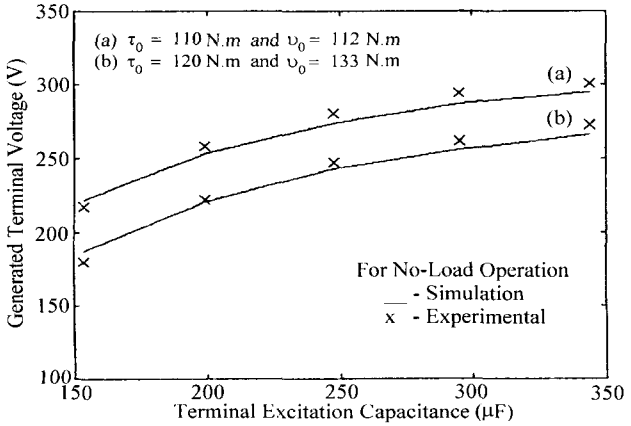

Fig.4 No load terminal voltage of SEIG vs. excitation capacitance

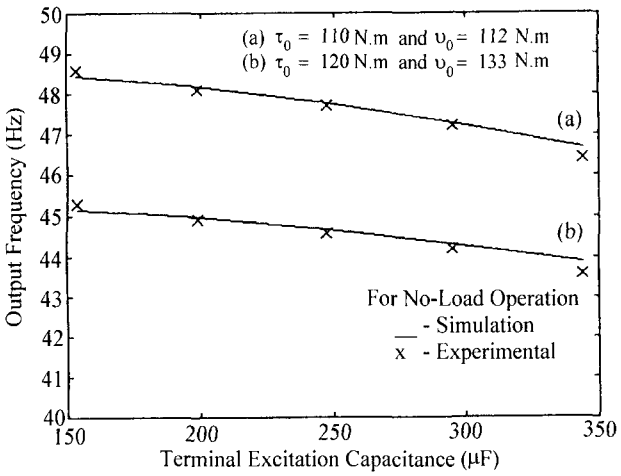

Fig.5 Output frequency of SEIG vs. excitation capacitance

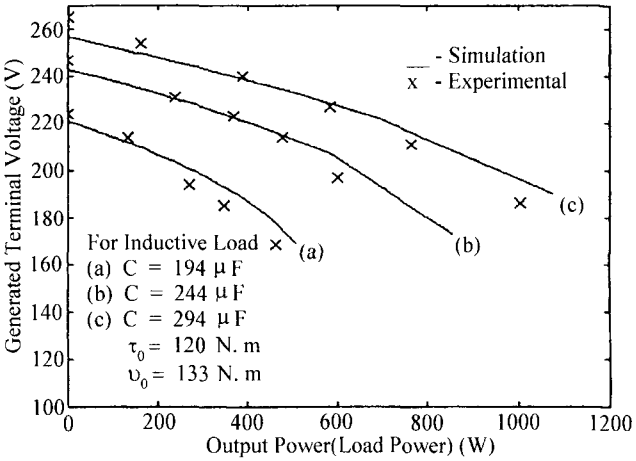

Fig.6 Terminal voltage of SEIG loaded by inductive load with different excitation capacitances

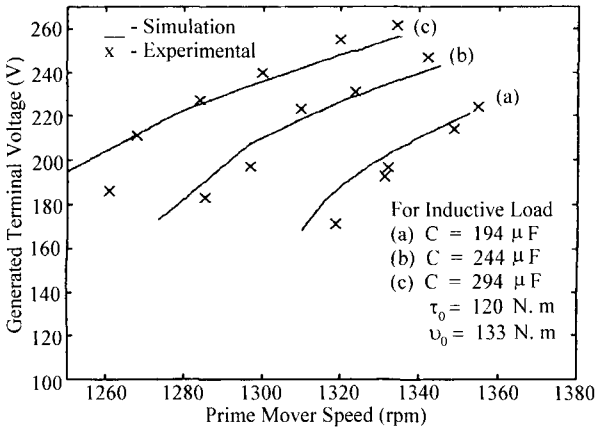

Fig.7 Terminal voltage of SEIG against its rotor speed with inductive load power variations

6.2 Operating performances of SEIG with CSPM

With a constant speed or relative rotor speed υ, the rotor impedance $\hat{Z}_r$, defined only as a function of the relative rotor speed υ in (A5) in Appendix and referred to in the stator winding side of the three-phase SEIG shown in Fig.3, can be represented with setting $G_0=0$, $G_1=R_2$, $G_2=-\upsilon$ and $G_3=1$. While the equivalent excitation capacitive reactance X_{SVC} of the SVC defined as (A4) in Appendix can be simplified and expressed only as a function of the fixed excitation capacitive reactance X_C by neglecting the inductive susceptance $[B_{TCR}(\sigma)=0]$ of the TCR and the TSC capacitive reactance ($X_{TSC}=0$), the result will be only the fixed excitation capacitive reactance (X_C/f^2).

For the three-phase SEIG driven by a CSPM with differing constant speeds of N=1400 rpm, N=1300 rpm and N=1250 rpm, Fig.8 shows the no-load generated terminal voltage vs. the excitation capacitance characteristics which are selected to be chosen above the minimum value required to build up the three-phase SEIG terminal voltage. The terminal voltage of the three-phase SEIG increases by increasing the capacitances of the excitation capacitor bank at a constant speed and also increases with increasing the CSPM speed. Fig.9 indicates the variations of the output frequency of the three-phase SEIG against its excitation capacitance with differing constant speeds of N=1400 rpm, N=1300 rpm and N=1250 rpm. The output frequency of the three-phase SEIG slightly changes with the increasing excitation capacitance as compared to the three-phase SEIG coupled by a VSPM shown in Fig.5 and increases linearly by increasing the CSPM speed. Fig.10 provides the load characteristics of the three-phase SEIG terminal voltage with the output power for a fixed capacitance of the excitation capacitor bank at a constant speed of N=1300 rpm when supplying an inductive load with a 0.8 lagging power factor. The terminal voltage variations are shown in the same figure for three values of excitation capacitances (C=244μF, 294μF and 344μF per-phase). The terminal voltage of the three-phase SEIG drops by increasing the inductive load. The output power increases with the CSPM more than with the VSPM. Fig.11 shows the output frequency variations of the three-phase SEIG against the inductive load power for an inductive load with 0.8 lagging power factor, a fixed excitation capacitance C=294μF and different values of constant speeds. The output frequency of the three-phase SEIG drops from the no load to the full load which means that the output frequency of the three-phase SEIG changes with the load power variations but with small variation ranges. The frequency variations increase with the inductive load power demand.

6.3 Setting voltage changes

The reference voltage changes are applied to test the PI controller parameters designed for the closed-loop terminal voltage regulation scheme. For an inductive load with 0.8 lagging power factor and a fixed excitation capacitance connected in parallel with the TCR, the digital simulation results and experimental results are depicted in Fig.12 and Fig.13 respectively.

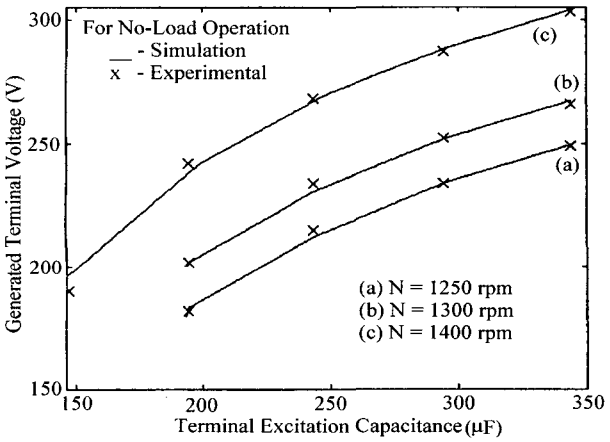

Fig.8 No load terminal voltage of SEIG vs. excitation capacitance

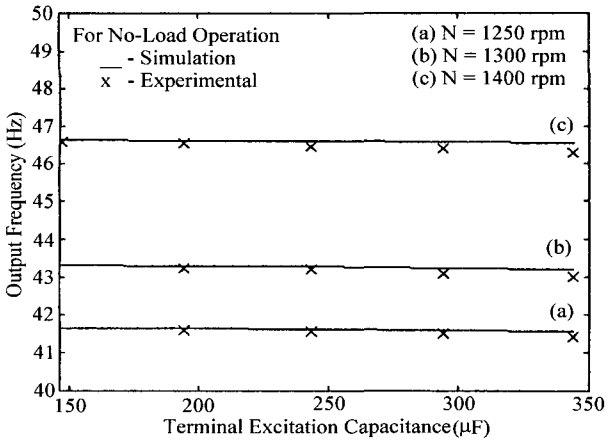

Fig.9 Output frequency of SEIG vs. excitation capacitance

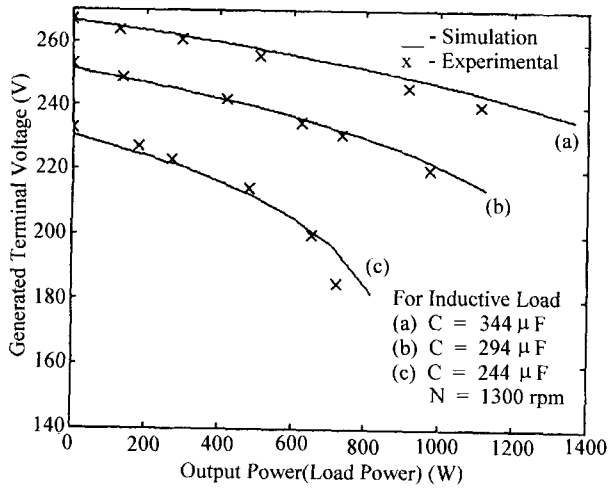

Fig.10 Terminal voltage of SEIG against output power

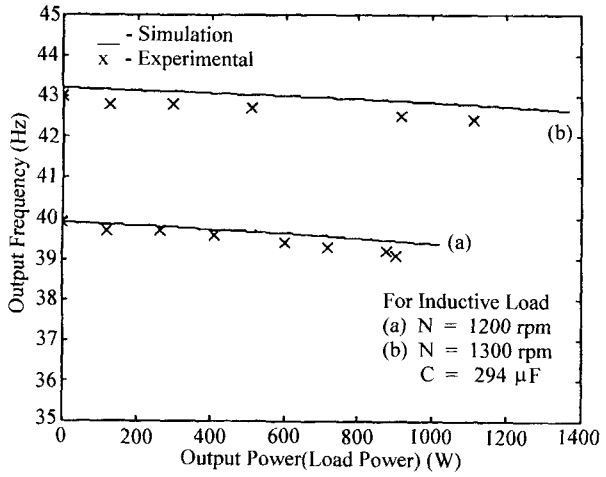

Fig.11 Output frequency of SEIG against output power

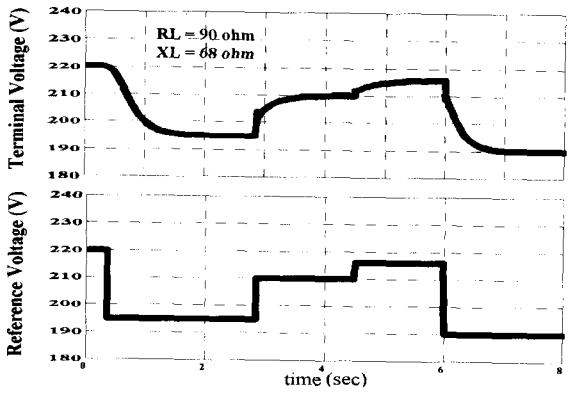

Fig.12 Three-phase SEIG terminal voltage and reference voltage responses in case of using SVC with inductive load

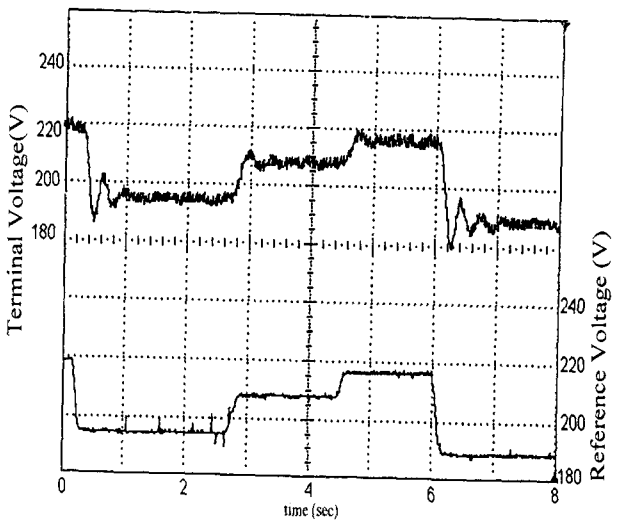

Fig.13 Three-phase SEIG experimental terminal voltage and reference voltage responses using SVC with inductive load

6.4 SEIG voltage regulation characteristics

With the fixed excitation capacitance parallel with the TCR, Fig.14 illustrates the terminal voltage response and the thyristor triggering delay angle response of the TCR due to the inductive load variations. The load impedance components have been increased from (R_L=90 Ohm and X_L=68 Ohm; i.e. less than the full load) to (R_L=1000 Ohm and X_L=750 Ohm i.e. no load) and then decreased to (R_L=100 Ohm and X_L=75 Ohm). For the full-load, the thyristor switched capacitor(TSC) is switched on with the fixed capacitor(FC) and TCR. Fig.15 illustrates the simulation results of SEIG terminal voltage response and thyristor triggering delay angle α of the TCR due to the inductive load variations with a 0.8 lagging power factor under the conditions of decreasing component values from (R_L=1000 Ohm and X_L=750 Ohm) to (R_L=75 Ohm and X_L=56 Ohm). At the same time, the simulation responses of the SEIG frequency and the speed of the variable-speed prime mover are depicted and magnified in Fig.16. The frequency mainly changes due to the variable speed prime mover and the full load. The controlled inductive susceptance of the TCR mainly depends on its triggering delay angle[13]. To minimize the harmonics, the TCR inductor and TSC capacitor are designed with the idea that the triggering delay angle of the TCR is small and closes to $\pi/2$ with respect to the zero crossing output voltage waveform[13]. The TSC unit switches on and off along

with the inductive load variations. The SEIG operation required a capacitive excitation current for building up its voltage so that the TCR current is very small when compared to the fixed capacitive excitation current, as is illustrated in Fig.17.

Fig.18 and Fig.19 depict the measured SEIG voltage regulation response and the TCR trigging angle response due to the inductive passive load variations under the above conditions mentioned of increasing and decreasing load impedance using the SVC composed FC in parallel with TCR and then switching on the TSC parallel to TCR.

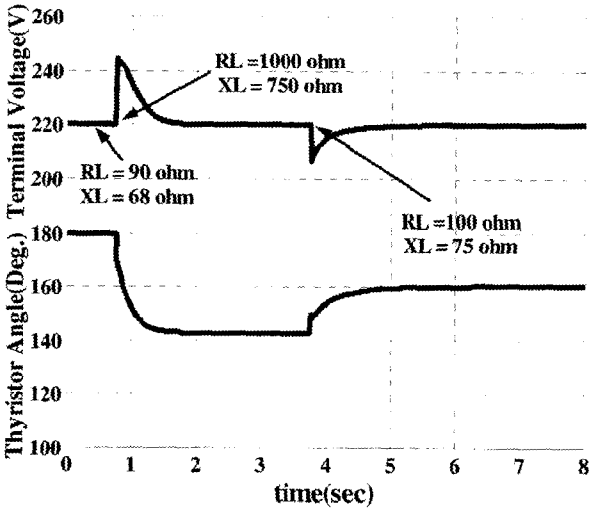

Fig.14 Terminal voltage and TCR thyristor triggering angle responses using SVC composed of FC and TCR

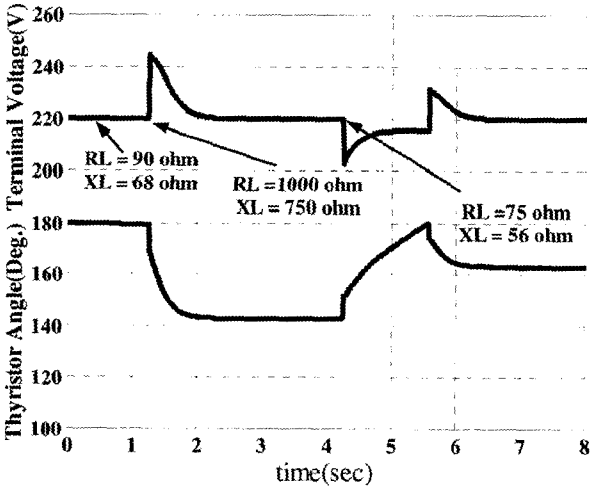

Fig.15 Terminal voltage and TCR thyristor triggering angle responses using SVC composed of FC, TSC and TCR.

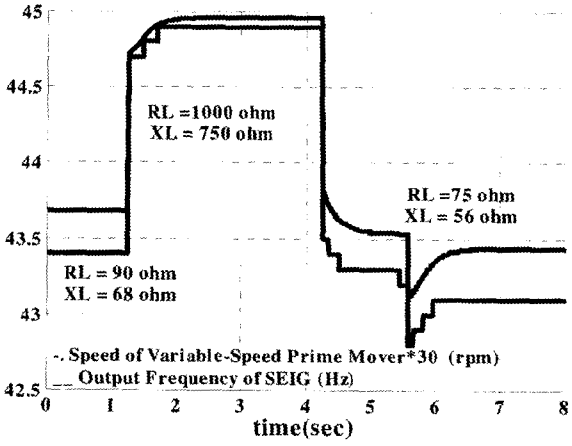

Fig. 16 Magnified output frequency response and speed response of VSPM using SVC(FC, TSC and TCR)

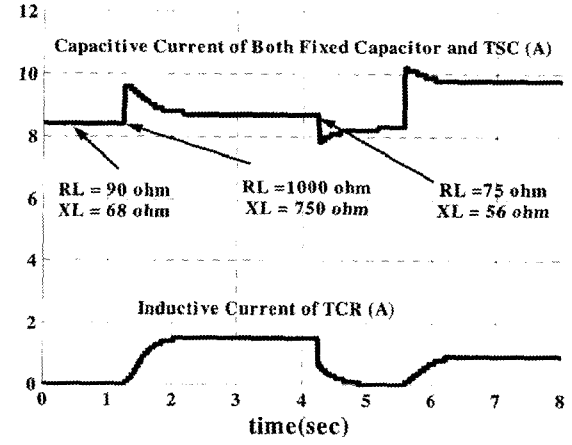

Fig.17 Capacitive current response of both FC and TSC and inductive current response of the TCR

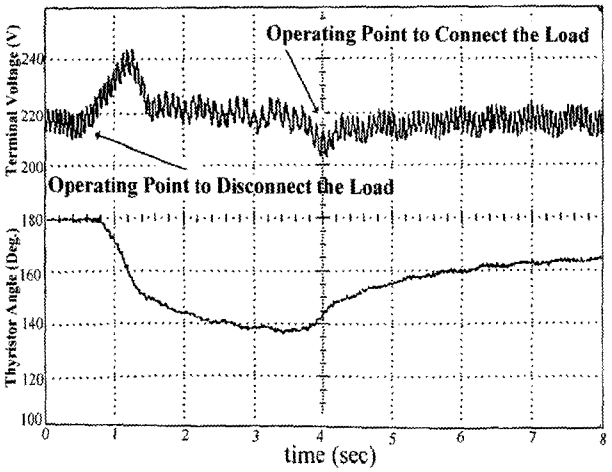

Fig.18 Experimental terminal voltage of SEIG and TCR thyristor triggering angle responses with FC and TCR

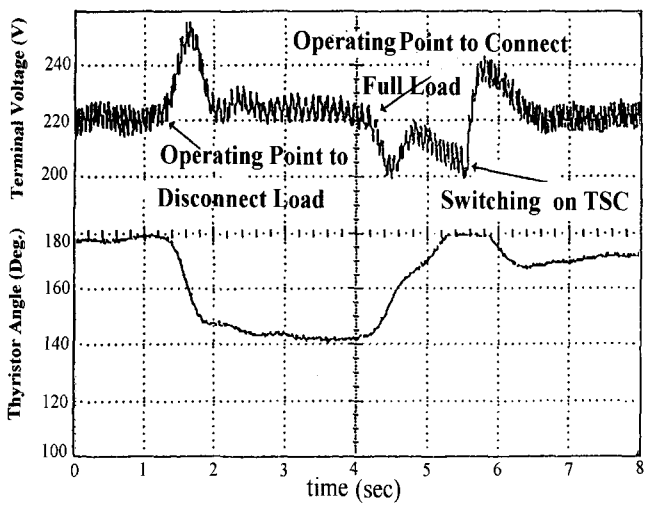

Fig.19 Experimental terminal voltage of SEIG and TCR thyristor triggering angle responses with FC, TSC and TCR

7. Conclusions

This paper introduced an effective algorithm for the steady-state analysis of operating performance evaluations based on the approximate equivalent circuit of the three-phase SEIG driven directly by a VSPM or a CSPM for the wind turbine or the micro gas turbine. In addition, this paper dealt with the SVC for the voltage regulation of the three-phase SEIG driven by the VSPM. The inductive load changes and reference voltage variations were applied to build and test the proposed SVC-based feedback control implementation system. A three-phase SEIG prototype set-up excited by SVC was established. The feasible experimental characteristics on the three-phase SEIG performance satisfactorily agreed with those obtained from the digital simulation results.

Appendix

$$\dot{Z}_{rm} = \frac{(jX_m)\dot{Z}_r}{\dot{Z}_r + jX_m} \quad \text{(A1)}$$

$$\dot{Z}_{mq} = \frac{R_1}{f} + jX_1 \quad \text{(A2)}$$

$$\text{and } \dot{Z}_{qr} = \left(\frac{-jX_{SVC}\left(\frac{R_L}{f} + jX_L\right)}{\frac{R_L}{f} + j(X_L - X_{SVC})}\right) \quad \text{(A3)}$$

$$\text{where, } X_{SVC} = \frac{X_C + X_{TSC}}{f^2 - (X_C + X_{TSC})B_{TCR}} \quad \text{(A4)}$$

$$\dot{Z}_r = \frac{R_2}{f - \upsilon} + jX_2 = \frac{\left(\frac{3E_1^2}{\omega_s} + \upsilon_0 R_2 f\right) + j(-\tau_0 + \upsilon_0 f)X_2 f}{(-\tau_0 + \upsilon_0 f)f} \quad \text{(A5)}$$

$$\text{or } \dot{Z}_r = \frac{(G_0 + G_1 f) + j(G_2 + G_3 f)X_2 f}{(G_2 + G_3 f)f}$$

$$\text{Let } \dot{Z}_{rmeq} = \dot{Z}_{qr} + \dot{Z}_{mq}$$

$$\dot{Z}_{rmeq} = \frac{R_1}{f} + jX_1 + \left(\frac{-jX_{SCV}\left(\frac{R_L}{f} + jX_L\right)}{\frac{R_L}{f} + j(X_L - X_{SCV})}\right) \quad \text{(A6)}$$

$$\dot{Z}_{rmeq} = \frac{(F_0 + F_2 f^2 + F_4 f^4) + j(T_0 + T_2 f^2)f}{(R_L f^3 - R_L X_{CE} B_{TCR} f) + j(X_L f^3 - X_L X_{CE} B_{TCR} f - X_{CE} f)}$$

where, $G_0=3E_1^2/\omega_s$,

$G_1=\upsilon_0 R_2$,

$G_2=-\tau_0$,

$G_3=\upsilon_0$,

$X_{CE}=X_C+X_{TSC}$,

$B_{TCR}(\sigma)=B_{TCR}=[\sigma-\sin(\sigma)]/\pi X_{TCR}$

$F_0=-R_L R_1 X_{CE} B_{TCR}$,

$F_2=R_L R_1+(X_1 X_L B_{TCR}+X_1+X_L)X_{CE}$,

$F_4=-X_L X_1$,

$T_0=-X_{CE}(R_L+R_1+R_L X_L B_{TCR}+R_1 X_L B_{TCR})$,

$T_2=R_1 X_L+R_L X_1$,

$C_0=G_0 T_0+G_2 X_2 F_0$,

$C_1=G_1 T_0+G_3 X_2 F_0$,

$C_2=G_0 T_2+G_2 X_2 F_2$,

$C_3=G_1 T_2+G_3 X_2 F_2$,

$C_4=G_2 X_2 F_4$,

$C_5=G_3 X_2 F_4$,

$A_0=-G_0 R_L X_{CE} B_{TCR}+G_2 F_0$,

$A_1=-G_1 R_L X_{CE} B_{TCR}+G_3 F_0$,

$A_2=G_2 X_2 X_{CE}(X_L B_{TCR}+1)+G_0 R_L+G_2 F_2$,

$A_3=G_3 X_2 X_{CE}(X_L B_{TCR}+1)+G_1 R_L+G_3 F_2$,

$A_4=-G_2 X_2 X_L+G_2 F_4$,

$A_5=-G_3 X_2 X_L+G_3 F_4$,

$D_0=G_0 F_0$, $D_1=G_1 F_0$,

$D_2=G_0 F_2-G_2 X_2 T_0$,

$D_3=G_1 F_2-G_3 X_2 T_0$,

$D_4=G_0F_4-G_2X_2T_2$,
$D_5=G_1F_4-G_3X_2T_2$,
$B_0=G_2(T_0-R_LX_2X_{CE}B_{TCR})-G_0X_{CE}(X_LB_{TCR}+1)$,
$B_1=G_3(T_0-R_LX_2X_{CE}B_{TCR})-G_1X_{CE}(X_LB_{TCR}+1)$,
$B_2=G_2(T_2+R_LX_2)+G_0X_L$,
$B_3=G_3(T_2+R_LX_2)+G_1X_L$,
$Y_0=A_0D_0$,
$Y_1=A_0D_1+A_1D_0$,
$Y_2=A_0D_2+A_1D_1+A_2D_0+B_0C_0$,
$Y_3=A_0D_3+A_1D_2+A_2D_1+A_3D_0+B_0C_1+B_1C_0$,
$Y_4=A_0D_4+A_1D_3+A_2D_2+A_3D_1+A_4D_0+B_0C_2+B_1C_1+B_2C_0$,
$Y_5=A_0D_5+A_1D_4+A_2D_3+A_3D_2+A_4D_1+A_5D_0+B_0C_3+B_1C_2+B_2C_1+B_3C_0$,
$Y_6=A_1D_5+A_2D_4+A_3D_3+A_4D_2+A_5D_1+B_0C_4+B_1C_3+B_2C_2+B_3C_1$,
$Y_7=A_2D_5+A_3D_4+A_4D_3+A_5D_2+B_0C_5+B_1C_4+B_2C_3+B_3C_2$,
$Y_8=A_3D_5+A_4D_4+A_5D_3+B_1C_5+B_2C_4+B_3C_3$,
$Y_9=A_4D_5+A_5D_4+B_2C_5+B_3C_4$,
$Y_{10}=A_5D_5+B_3C_5$,

References

[1] A.K.Aljabri and A.I.Alolah, "Capacitance Requirement for Isolated Self-Excited Induction Generator", IEE Proceedings, Part B, Vol.137, No.3, pp.154-159, May, 1990.

[2] S.P.Singh, M.P.Jain and Bhim Singh, "A New Technique for Analysis of Self-Excited Induction Generator", Electric Machine and Power Systems, Vol.23, pp.647-656, 1995.

[3] Li Wang and Lian-Yi Su, " Effects of Long-Shunt and Short-Shunt Connections on Voltage Variations of A Self-Excited Induction Generator", IEEE Trans. on Energy Conversion, Vol.12, No.4 pp.368-374, December, 1997.

[4] S.Rajakarvna and R.Bonert, "A Technique for The Steady state Analysis of Self-Excited Induction Generator with Variable Speed", IEEE Trans. on Energy Conversion, Vol.8, No.4 pp.757-761, December, 1993.

[5] Tarek Ahmed, Osamu Noro, Koji Sato, Eiji Hiraki and Mutsuo Nakaoka "Single-Phase Self-Excited Induction Generator with Static VAR Compensator Voltage Regulation for Simple and Low Cost Stand-Alone Renewable Energy Utilizations" KIEE International Transactions on Power Engineering, Vol.3-A, No.1, pp.17-34, 2003.

[6] Michael B. Brennen and Alberto Abbondanti," Static Exciters for Induction Generator" IEEE Trans. on Industry Applications, Vol.IA-13, No.5, September/ October, 1977.

[7] Marcos S. Miranda, Renato O. C. Lyra and Selenio R. Silva, "An Alternative Isolated Wind Electric Pumping System Using Induction Machines", IEEE Trans. on Energy Conversion, Vol.14, No.4 pp.1611-1616, December, 1999.

[8] Ermis, H.B.Erton, M.Demirekler, B.M.Saribatir, Y.Uctvg, M.E.Sezer and I.Cadirici," Various Induction Generator Schemes for Wind-Electricity Generation", Electric Power Systems Research, Vol.23, pp.71-83, 1992

[9] A.A.Shaltout and M.A.Adel-Halim, "Solid State Control of Wind-Driven Self-Excited Induction Generator", Electric Machines and Power Systems, Vol.23, pp.571-582,1995

[10] E. Suarez and G. Bortolotto, "Voltage-Frequency Control of A Self-Excited Induction generator", IEEE Trans. on Energy Conversion, Vol.14, No.3 pp.394-401, September, 1999.

[11] R. Leidhold, G. Garcia and M.I. Valla, "Induction generator Controller Based on the Instantaneous Reactive Power Theory", IEEE Trans. on Energy Conversion, Vol.17, No.3 pp.368-373, September, 2002.

[12] M. Naidu and J. Walters, "A 4-kW 42-V Induction-Machine-Based Automotive Power Generation System With a Diode Bridge Rectifier and a PWM Inverter", IEEE Trans. on Industry Applications, Vol.39, No.5 pp.1287-1293, September/October, 2003.

[13] IEEE Special Stability Controls Working Group Report, "Static VAR Compensator Models for Power Flow and Dynamic Performance Simulation ", IEEE Transactions on Power Systems, Vol.9, No.1, February, 1994.

Tarek Ahmed received his M.Sc. degree in electrical engineering from the Electrical Engineering Department, Faculty of Engineering, Assiut University, Egypt in 1998. He is working a staff member as an assistant lecturer in the Electrical Engineering Department, Faculty of Engineering, Assiut University, Assiut, Egypt. He is currently a Ph. D. candidate student with the Power Electronic System and Control Engineering Laboratory, the Division of Electrical and Electronic Systems Engineering, the Graduate School of Science and Engineering, Yamaguchi University, Yamaguchi, Japan. He has received the Paper Awards from the Institute of Electrical Engineers of Japan (IEE-J) in 2003 and in 2004. His research interests are in the new applications of the advanced high frequency resonant circuits and systems with the renewable energy related soft switching PWM rectifier and sinewave PWM inverter power conditioner.

Mr. Ahmed is a student-member of the Institute of Electrical and Electronics Engineers of USA (IEEE-USA), the Institute of Electrical Engineering and Installation of Engineers (IEIE-Japan),

he Institute of Electrical Engineers (IEE-Japan) and Japan nstitute of Power Electronics (JIPE).

Katsumi Nishida received the B.S., and M.S. degrees in electrical engineering from the Tokyo Institute of Technology, Tokyo in 1976, 1978, respectively. He received the Ph.D. degree from the Division of Electrical and Electronic Systems Engineering, the Graduate School of Science and Engineering, Yamaguchi University, Yamaguchi, Japan in 2002. He is engaged in research on the power factor correction of the PWM converter and the current control of the three-phase active power filter with the dead-beat technique and the adaptive signal processing technique.

Dr.-Eng. Nishida is a member of the Institute of Electrical and Electronics Engineers of USA (IEEE-USA), the Institute of Electrical Engineers of Japan (IEE-Japan) and Japan Institute of Power Electronics (JIPE).

Mutsuo Nakaoka received his Dr.-Eng. degree in Electrical Engineering from Osaka University, Osaka, Japan in 1981. He joined the Electrical and Electronics Engineering Department of Kobe University, Kobe, Japan in 1981 and served as a professor of the Department of Electrical and Electronics Engineering, the Graduate School of Engineering, Kobe University, Kobe, Japan until 1995. Now he is working a professor in the Electrical and Electronics Engineering Department, the Graduate School of Science and Engineering, Yamaguchi University, Yamaguchi, Japan. His research interests include application developments of power electronics circuits and systems. He has received more than ten Awards such as the 2001 premium prize paper award from IEE-UK, the 2001 and 2003Best Paper Award from IEEE-IECON, the 2000 third paper award from IEEE-PEDS, 2003 James Melcher Prize Paper award from IEEE-IAS. He is now a chairman of IEEE Industrial Electronics Society Japan Chapter.

Prof. Dr.-Eng. Nakaoka is a member of the Institute of Electrical Engineering Engineers of Japan, Institute of Electronics, Information and Communication Engineers of Japan, Institute of Illumination Engineering of Japan, European Power Electronics Association, Japan Institute of Power Electronics, Japan Society of the Solar Energy, Korean Institute of Power Electronics, IEE-Korea and IEEE.